

Preliminary SuperTIGER Abundances of Galactic Cosmic-Rays for the Charge Interval Z=41-56 and Prospects for SuperTIGER-2

N.E. Walsh¹, W.R. Binns, M.H. Israel, R.P. Murphy, B.F. Rauch, J.E. Ward

*Washington University
St. Louis, MO 63130, USA
E-mail: newalsh@wustl.edu*

T.J. Brandt, J.T. Link, J.W. Mitchell, T. Hams, K. Sakai, M. Sasaki

*NASA Goddard Space Flight Center
Greenbelt, MD 20771, USA*

A.W. Labrador, R.A. Mewaldt, E.C. Stone

*California Institute of Technology
Pasadena, CA 91125, USA*

M.E. Wiedenbeck

*Jet Propulsion Laboratory, California Institute of Technology
Pasadena, CA 91125, USA*

C.J. Waddington

*University of Minnesota
Minneapolis, MN 55455, USA*

The SuperTIGER (Trans-Iron Galactic Element Recorder) instrument was launched from Williams Field, Antarctica on December 8, 2012 and flew for 55 days at a mean altitude of 125,000 feet on a long-duration balloon flight. SuperTIGER measured the relative abundances of Galactic cosmic-ray nuclei with high statistical precision and well resolved individual element peaks in the charge range Z=10-40. In addition, SuperTIGER made exploratory measurements of the relative abundances up to Z=56. Although the statistics are low for charges greater than Z=40, we will show how the relative abundances of charges Z=40-56 compare to those reported by HEAO3. A second flight, SuperTIGER-II, is planned for December 2017. As SuperTIGER-II will fly during solar minimum, we estimate a ~50% increase in the particles collected per unit time as compared to SuperTIGER-I. With the combined data sets of SuperTIGER-I and II we will improve statistics in the Z=30-40 range and measure individual elemental abundances up to Z=56.

*35th International Cosmic Ray Conference - ICRC2017
10-20 July, 2017
Bexco, Busan, Korea*

¹Speaker

1. Introduction

The SuperTIGER (ST) instrument has undergone minor improvements and refurbishments since its first, 55 day flight (ST-I) in December, 2012 (Figure 1) and is planned to launch from McMurdo Station, Antarctica on a second long-duration balloon flight (ST-II) during the Austral summer of 2017-18. The instrument design is focused on making well resolved individual element abundance measurements of ultra-heavy-Galactic cosmic rays (UHGCR). The data produced is expected to improve the statistics of existing ST-I measurements made in the charge range Z=30-40 and to allow the first accurate measurements of individual elements in the charge range Z=40-56.

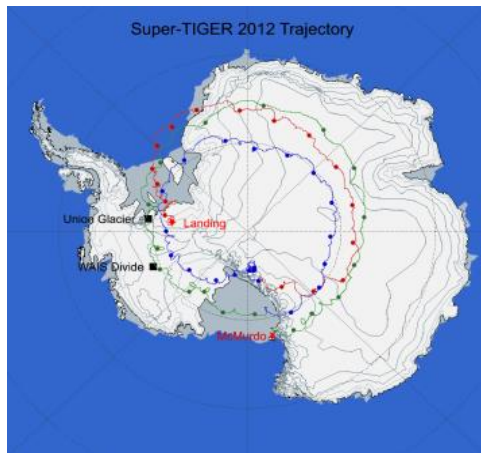


Figure 1: SuperTIGER 2012 flight path. Completed 2.75 rotations about the South Pole.

ST-I collected excellent data on over 5 million GCR ^{26}Fe nuclei (about 44 equivalent days of data) and ST-II is hoped to achieve a similar number of events. The ST-II will occur during solar minimum, where a \sim 50% increase in the cosmic-ray flux is expected over what ST-I saw. If ST-II flies for 30 days then the amount of data collected is expected to be equivalent to \sim 44 days of effective data collected by ST-I.

The data analysis method used for ST-II will be similar to that utilized after the ST-I flight. When data from the two flights are combined we can expect sufficient improvement in the statistics such that the elements greater than $_{40}\text{Zr}$ can be measured. The prospects for this measurement can be shown by comparing the exploratory ST-I Z>40 measurements with those made in this range by the Heavy Nuclei Experiment aboard the third High-Energy Astronomy Observatory satellite (HEAO-3-HNE).

2. Instrument Overview

The ST-I instrument was recovered from Antarctica during the Austral summer of 2014-15 and was found to be in overall excellent condition. It was decided that the original instrument could be flown again for a second flight, ST-II, and so the ST-I&II instrumentation is essentially identical, save some minor refurbishments and improvements. In addition, the high voltage power supply and on-board data recording system have been redesigned.

The instrument consists of two nearly identical modules, each containing seven stacked detectors (Figure 2). From top to bottom, in each module there is a plastic scintillation detector (S1), a scintillating optical fiber hodoscope layer (H1), a silica-aerogel Cherenkov detector (C0), an acrylic Cherenkov detector (C1), a second scintillation detector (S2), a second hodoscope layer (H2), and a third scintillation detector (S3). The signals from the S and C detectors are used in combination to measure both the charge and kinetic energy of cosmic rays that pass through the entire stack. The H layers are used to determine each cosmic ray's trajectory through the instrument, allowing angle corrections and area mapping to be performed.

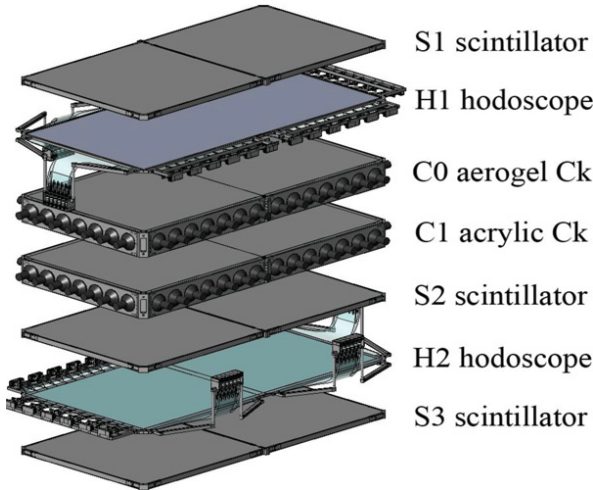


Figure 2: SuperTIGER detector stack. One module shown.

The SuperTIGER instrument is designed to measure UHGCR, which are both rare and interact readily, so maximizing statistics and minimizing particle interactions are priorities. To achieve these priorities, maximum altitude and minimum interactions are attained by using light materials with low interaction cross-sections throughout the instrument. High statistics are also achieved by the instrument's large physical acceptance geometry. Each module has an active area of 1.16 m by 2.4 m and together give the instrument a combined effective geometry factor of 3.9 m²sr (after interactions are removed using ³⁴Se nuclei as a reference) (Binns et al., 2014).

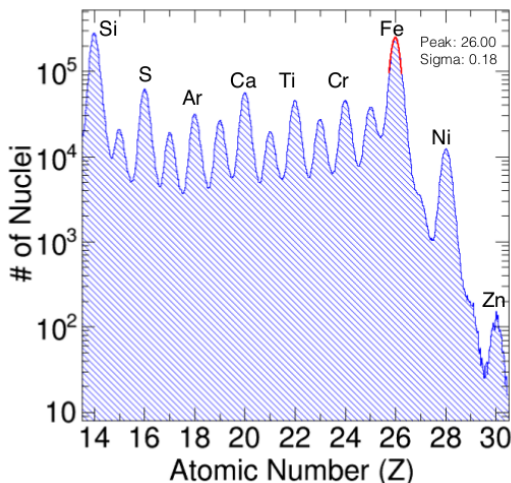


Figure 3: SuperTIGER Z=14-30 elemental abundances. Individual element peaks clearly visible.

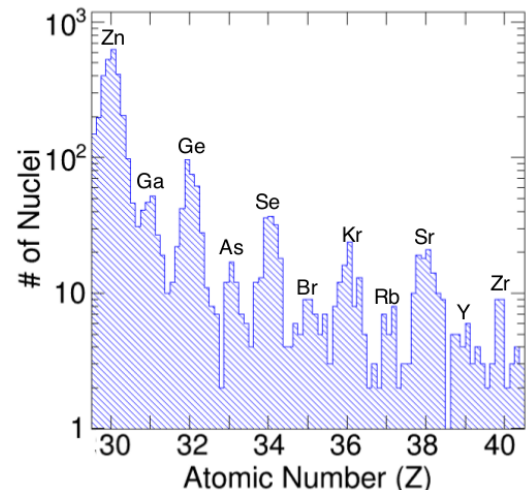


Figure 4: SuperTIGER Z=30-40 elemental abundances. Low statistics but individual element peaks still visible.

3. SuperTIGER Z=30-40

ST-I made the best UHGCR abundance measurements to date in the charge range Z=30-40 (Murphy et al., 2016). Individual element peaks are clearly resolved from ^{14}Si to ^{30}Zn (aside from ^{27}Co and ^{29}Cu) with ^{26}Fe having a sigma of 0.18 cu (Figure 3). Although the statistics are much lower, individual element peaks are also well resolved from ^{30}Zn to ^{40}Zr (Figure 4).

When plotting the Galactic-cosmic-ray-source (GCRS) abundances relative to the solar system (SS) abundances (Lodders, 2003), patterns for the preferential acceleration of refractory elements (dust) over the volatiles (gas) and for a mass dependence in GCR volatile acceleration are suggested (Figure 5). When instead the GCRS abundances are plotted relative to a mixture of ~80% SS material with ~20% massive star material (MSM) the refractories and volatiles separate completely and the mass trend of the acceleration of both the refractories and volatiles emerges (Figure 6). The ST results combined with those from TIGER (Rauch et al., 2009) and HEAO-3-C2 (Engelmann et al., 1990) show that refractories are accelerated preferentially over volatiles by a factor of ~4 and that the GCR source material is a mixture of massive star material and normal interstellar medium material.

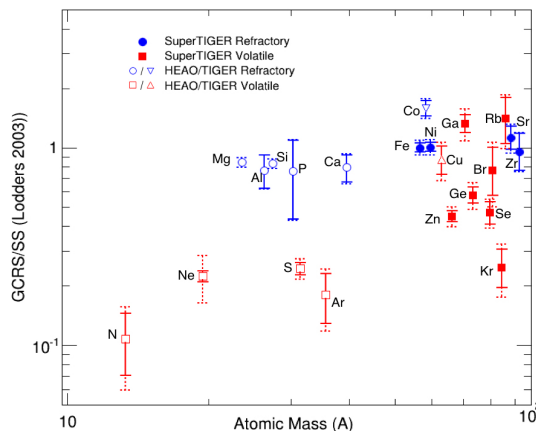


Figure 5: Dependence on A of GCRS material relative to SS. Refractories and volatiles not clearly separated.

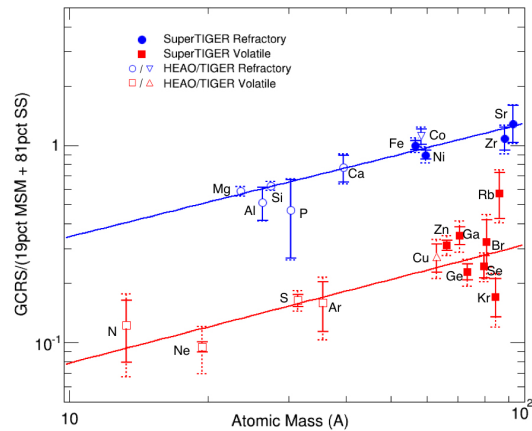


Figure 6: Dependence on A of GCRS material relative to mixture of MSM with normal SS material. Refractories preferred over volatiles by factor of ~4.

To achieve excellent charge resolution over wide charge and energy ranges, two complementary methods were used in the data analysis. The first method utilizes the signals from the two Cherenkov detector layers C0 and C1. The C0 material, aerogel, has an index of refraction $n=1.04$ ($n=1.025$ in one half module) while the C1 material, acrylic, has an index $n=1.49$. Because the Cherenkov signal only occurs when the particle velocity exceeds $\beta=1/n$, this method can only be used for particles with energies greater than 2.5 GeV/nucleon (or 3.3 GeV/nucleon for $n=1.025$), where the C0 detector “turns on”. Even though the charge determination made via the combined Cherenkov method yields better charge resolution, for lower energies, where C0 does not give a Cherenkov signal, a method using a combination of scintillation detector signals with the C1 signal must be used. This method works down to energies of ~350 MeV/nucleon,

where the C1 detector turns on, which is sufficiently low to include most UHGCR that pass through the instrument.

These charge identification methods can be illustrated with cross plots of S1 vs. C1 (Figure 7) for energies below the C0 threshold, and C1 vs. C0 signals (Figure 8) for energies above the C0 threshold. One can easily see the charge bands that emerge when plotting the signals in this fashion, and it is the clear separation between these bands that can be used to determine charge for all particles passing through the instrument. The complementary nature of these methods is clear when comparing the Above and Below C0 regions in these two plots. An approximation of the C0 threshold energy line is drawn in red on both the C1 vs. C0 and the S1 vs. C1 plots, and it can be seen that, although the Above C0 region to the right of the line is very dense on the S1 vs. C1 plot, the particles in the same energy region to the right of the line on the C1 vs. C0 plot spread out nicely into charge bands. The Below C0 region is similarly dense on the left of the line in the C1 vs. C0 plot and is resolved on the left of the line in the S1 vs. C1 plot.

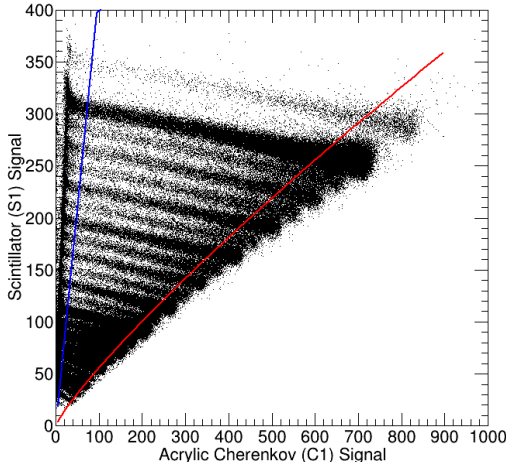


Figure 7: Below C0 method (S1 vs. C1). Blue line is low energy cut. Red line is approximate C0 threshold energy. Particles to the left are well resolved.

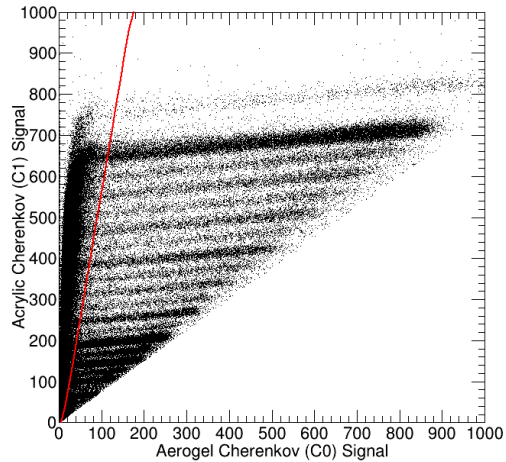


Figure 8: Above C0 method (C1 vs. C0). Red line is approximate C0 threshold energy. Particles to the right are well resolved.

For the Above C0 method (C1 vs. C0), charge determination is fairly straightforward. In the analysis of Murphy et al. (2016) a second order polynomial was fit to the ^{26}Fe charge band for several different angle bins. The Cherenkov light produced by a charged particle (and therefore the Cherenkov detector signal) is proportional to Z^2 , so that the parallel C1 vs. C0 charge bands are separated by such a factor. If one then finds the functional form of one line (the iron line in this case) one can solve for the charge of any Above C0 particle from its C1 and C0 detector signals.

The Below C0 method (S vs. C1) has a more complicated dependence as the scintillation light produced by a charged particle does not have a straightforward dependence on the charge. To achieve better charge resolution, the analysis is done separately for both S1 vs. C1 and for S2 vs. C1 and then the charge determination from both signals is averaged. For different angle bins, one fits multiple charge bands with second order polynomials and also spans the S vs. C1 space with lines of constant energy. The intersections between the charge contours and lines of constant energy can

be found, and the scintillator signal as a function of charge for each energy can be fit with a model of scintillation light yield (Murphy used the Voltz model). Finding the functional parameters of each fit reveals the dependence of these parameters on energy. Once this dependence is known, the fitting function can be solved for Z for any particle. Relating particle energy to the C1 signal makes it possible to solve for Below C0 particle charges from S and C1 signals.

The charges are determined for events from the Above and Below C0 energy regions with these methods. Interaction cuts and velocity corrections appropriate to each of these energy regions are applied and Above and Below C0 charge determinations are finalized. The resulting combined Above and Below C0 charge histograms (Figures 3 & 4) have well resolved peaks.

4. SuperTIGER Z=41-56

In order to analyze the UHGCR higher than $_{40}\text{Zr}$, the above method for charge determination must be modified as it is optimized for the Z=30-40 range. The most important modification is that the interaction cuts applied to achieve the desired resolution on the Z=30-40 range are loosened appropriately. Heavier particles undergo interactions much more readily and therefore lack the statistics that would allow for harsher cuts. Once the cuts are loosened, the preliminary Above and Below C0 combined histogram features charge peaks all the way up to Z=60 (Figure 9) and a comparison to HEAO-3-HNE data (Figure 10) (Binns et al., 1989) can be made.

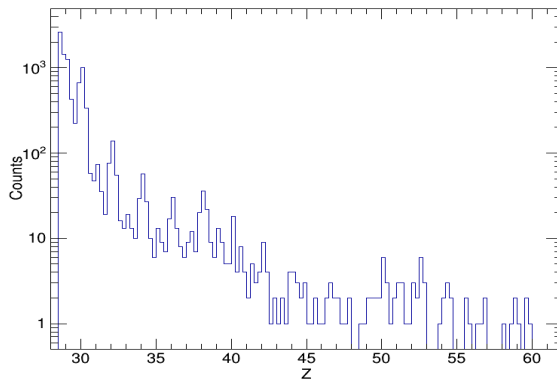


Figure 9: Preliminary ST elemental abundances for Z=30-60. Individual element abundances for Z=30-60. Only even-odd charge pairs visible.

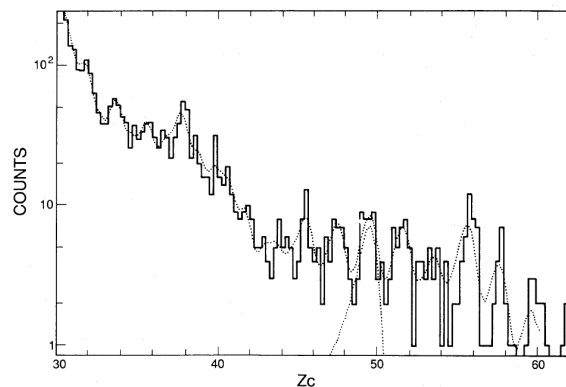


Figure 10: HEAO-3-HNE elemental abundances for Z=30-60. Only even-odd charge pairs are resolved.

Comparing the ST balloon-altitude measurements with the HEAO-3 space-based measurements requires additional analysis. The ST instrument abundances must be corrected for atmospheric nuclear interactions and energy losses to give top-of-the-atmosphere (TOA) abundances. Then, as HEAO-3-HNE can only resolve combined even and odd charge pairs, the even and odd individual ST element peaks were added together, normalized and compared to HEAO-3-HNE abundances (Table 1 & Figure 11). Overall the comparison seems quite consistent. The SuperTIGER and HEAO-3-HNE even-odd abundances seem to agree nicely for the Z=30-60 range. The largest deviation occurs for the combined Z=55&56 peak. This agreement is evidence that ST-II has good prospects for improving upon the above Z=40 abundance measurements of ST-I by providing an increase in statistics.

Charge	Raw Counts	Fe = 10 ⁶	plus/min	TOA Fe=10 ⁶	plus/min	HEAO Fe=10 ⁶	plus/min
30	2280	556					
31-32	461	112.4					
33-34	178	43.4	3.4/3.2	49.2	4.2/4.1	51.2	3.7
35-36	103	25.1	2.8/2.5	28.7	3.7/3.2	35.1	3
37-38	121	29.5	3.0/2.7	37.6	4.2/3.7	39.6	3.1
39-40	56	13.7	2.2/1.8	17.4	3.1/2.6	22.2	2.6
41-42	43	10.5	2.0/1.6	14.1	2.9/2.3	15.4	2.1
43-44	18	4.4	1.4/1.0	5.6	2.2/1.5	4.6	1.2
45-46	10	2.4	1.2/0.7	2.7	1.9/1.2	6.7	1.4
47-48	14	3.4	1.3/0.9	4.6	2.2/1.5	5.5	1.3
49-50	19	4.6	1.4/1.0	7.1	2.6/1.9	6.3	1.5
51-52	14	3.4	1.3/0.9	5.5	2.4/1.7	5.2	1.4
53-54	19	4.6	1.4/1.0	8.4	2.8/2.0	3.1	1.2
55-56	3	0.7	0.8/0.4	1.2	1.6/0.8	6.3	1.6
57-58	5	1.2	1.0/0.5	2	2.0/1.0	3.5	1.3
59-60	7	1.7	1.1/0.6	3.2	2.3/1.3	1.5	1.1

Table 1: ST even and odd charge peaks are propagated to TOA and summed to compare to HEAO-3-HNE charge pairs.

5. Impact of Solar Modulation

After comparing ST-I elemental abundances with those of HEAO-3-HNE it is clear that the second flight ST-II will significantly improve the measurements above Z=40. Flying an almost identical instrument will provide equally well resolved charge determinations that will add to the existing peaks from ST-I and make them more well defined. SuperTIGER achieved a 55 day flight and, due to the necessity to rely on telemetered data, effectively 44 days of measurement in 2012-13. In this time, it was able to measure more than 5 million GCR Fe nuclei. In the 2017-18 Austral summer ST-II will fly during solar minimum, when there will be lower solar modulation, allowing more GCR events per unit time to be collected (Figure 12, R.A. Mewaldt, private communication). In 2012-13, during the ST-I flight, the solar modulation was \sim 500 MV, blocking 43% of the GCR flux seen in the 2009-10 solar minimum with a modulation factor of \sim 250 MV. If the modulation reaches 250 MV as in 2009, we expect to measure \sim 43% more GCR per unit time and if the modulation reaches 125 MV we should see \sim 77% more GCR. So it is very reasonable to assume a 50% increase in the cosmic-ray flux we will see with ST-II over ST-I. Thus, ST-II will only need to fly for 30 days to measure the same number of particles that ST-I did in 2012-13.

6. Conclusions

ST-II will increase our total ST statistics and allow us to make more accurate abundance measurements of the UHGCR that could yield more information about the origins of GCR. Concrete measurements above Z=40 would allow us to add additional points to Figure 6, stretching the lever arm on the mass trend into a higher mass region. ST-I data showed that an \sim 80% SS to \sim 20% MSM mixture made sense of the refractory over volatile preferential acceleration in the GCR, and pointed to GCR having a significant origin in OB associations. However, with more points to add in the higher mass region we may see changes in this plot that point to other GCR sources, such as binary neutron star mergers (Just et al., 2015).

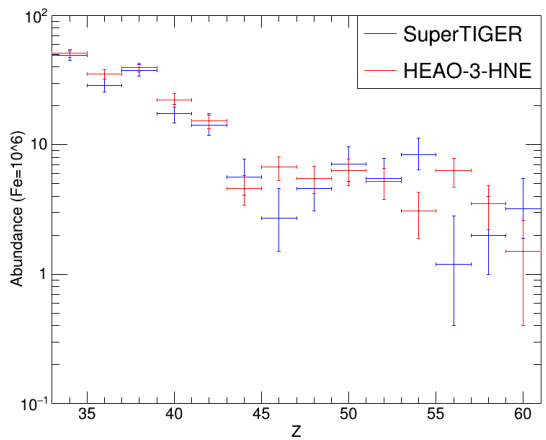


Figure 11: ST and HEAO-3-HNE charge pair abundances agree quite well within statistics. ST error bars follow Gehrels confidence limits for small numbers of astrophysical events.

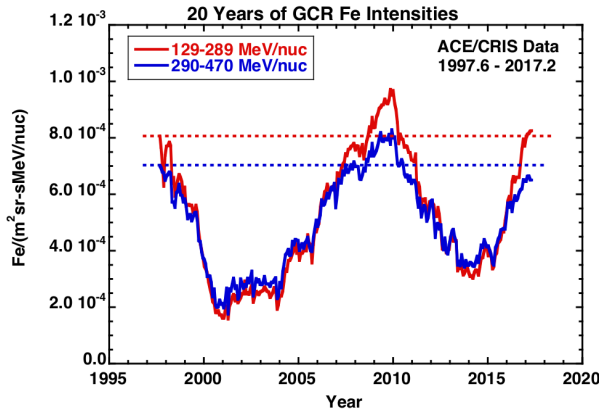


Figure 12: Cosmic-ray Fe flux changing through solar cycle. ST-I flew 2012-13 and ST-II will fly 2017-18. Cosmic-ray flux will be much higher for ST-II than for ST-I.

References

- [1] W.R. Binns et al., The SuperTIGER Instrument: Measurements of Elemental Abundances of Ultra-Heavy Galactic Cosmic Rays, *ApJ*, 788 (2014) 18-28.
- [2] R.P. Murphy et al., Galactic Cosmic Ray Origins and OB Associations: Evidence from SuperTIGER Observations of Elements 26 Fe Through 40 Zr, *ApJ*, 831 (2016) 2083-2088.
- [3] K. Lodders, Solar System Abundances and Condensation Temperatures of the Elements, *ApJ*, 591 (2003) 1220-1247.
- [4] B.F. Rauch et al., Cosmic Ray origin in OB Associations and Preferential Acceleration of Refractory Elements: Evidence from Abundances of Elements 26 Fe through 34 Se, *ApJ*, 697 (2009) 2083-2088.
- [5] J.J. Engelmann et al., Charge composition and energy spectra of cosmic-ray nuclei for elements from Be to NI - Results from HEAO-3-C2, *A&A*, 233 (1990) 96-111.
- [6] W.R. Binns et al., Abundances of Ultraheavy Elements in the Cosmic Radiation: Results from HEAO 3, *ApJ*, 346 (1989) 997-1009.
- [7] N. Gehrels, Confidence Limits for Small Numbers of Events in Astrophysical Data, *ApJ*, 303 (1986) 336-346.
- [8] O. Just et al., Comprehensive Nucleosynthesis Analysis for Ejecta of Compact Binary Mergers, *Monthly Notices of the Royal Astronomical Society*, 000 (2015) 1-30.